Evaluation of surface/interface quality, microstructure and mechanical properties of hybrid additive-subtractive aluminium parts

Bhaduri, Debajyoti; Penchev, Pavel; Essa, Khamis; Dimov, Stefan; Carter, Luke; Pruncu, Catalin; Pullini, Daniele

DOI:
10.1016/j.cirp.2019.04.116

Contents lists available at SciVerse ScienceDirect

CIRP Annals Manufacturing Technology

Journal homepage: www.elsevier.com/locate/cirp

Evaluation of surface / interface quality, microstructure and mechanical properties of hybrid additive-subtractive aluminium parts

Debajyoti Bhaduri [a,b,*], Pavel Penchev [b], Khamis Essa [b], Stefan Dimov [b], Luke N. Carter [c], Catalin I. Pruncu [b,d], Daniele Pullini [e]

[a] School of Engineering, Cardiff University, Queen's Buildings, The Parade, Cardiff, CF24 3AA, UK
[b] Department of Mechanical Engineering, School of Engineering, University of Birmingham, Edgbaston, Birmingham, B15 2TT, UK
[c] School of Metallurgy and Materials, University of Birmingham, Edgbaston, Birmingham, B15 2TT, UK
[d] Department of Mechanical Engineering, Imperial College London, South Kensington Campus, London, SW7 2AZ, UK
[e] C.R.F ScPA., Sede legale e amministrativa: Strada Torino, 50, 10043 Orbassano (TO), Italy

Submitted by T.H.C. Childs (1), Leeds, UK

A disadvantage of selective laser melting (SLM) processes for the manufacture of large parts is their slow build time per unit volume. A hybrid route is to generate core simple shapes traditionally, for example by machining, followed by adding final features by SLM. Here the mechanical integrity of such hybrid parts is studied, choosing the building of AlSi10Mg by SLM on a machined AA6082 base, in the shape of a tensile test piece, as a simple example. These materials are chosen for their relevance to lightweight parts. As-built parts fail at the SLM/machined interface but standard heat treatments transfer failures to the machined material. Optimised SLM processing conditions and microstructures of the SLM and interfacial regions are reported.

Additive manufacturing, selective laser melting (SLM), aluminium

1. Introduction

Over the past two decades laser based additive manufacturing (AM) has matured to a level where it can be considered as a viable alternative for producing net shape metal components in a single processing step for relatively small markets, mainly for prototyping and small batch manufacture. These are niche markets and the technology still does not meet the requirements of mass market applications that would make it an ideal candidate to fulfil the aims of Industry 4.0 [1]. One way to exploit the benefits of design freedom of AM as well as the shorter process time of subtractive manufacturing (SM) is to produce geometrically simple sections via SM (e.g. machining), followed by more complex AM structures built upon them [2]. The finished parts can then be post-processed (via further machining, mechanical and/or laser polishing, heat treatment etc.), depending on their functional requirements. Manufacture of such parts renders integrated functionalities for a broad range of industrial applications, e.g. aerospace, automotive, railway, electronic and biomedical sectors. A research need is to establish the mechanical integrity of parts built in this way. This paper describes fabrication and testing of hybrid AM-SM parts in the form of tensile test pieces. AA6082-T6 alloy is chosen as the SM half of the part (the preform) and AlSi10Mg powder is used for building the AM half, by selective laser melting (SLM) [3]. These alloys, of similar composition, are strong candidates for commercial application. Results are presented for optimisation of SLM parameters and the testing of as-built and heat treated parts. Properties equivalent to entirely SM parts are obtained [4].

2. Experimental details

In an initial experimental phase, 24 preform cubes (10 × 10 × 10 mm) were slot-milled from an AA6082-T6 aluminium block, purchased off-the-shelf. SLM structures (10 × 10 × 10 mm) were then built in-house on top of the preforms. These were held in modular devices, Fig. 1(a), that were developed and validated in a previous study for integrating laser-based powder bed fusion processes with other complementary pre-processing (machining or metal injection moulding) and post-processing technologies in hybrid manufacturing platforms [5]. They ensured a positional accuracy of the AM sections on the preforms between ~10-21 µm.

The SLM sections were produced using gas atomised AlSi10Mg powder, supplied by LPW Technology Ltd, with a particle size range of ~20-63 µm. Details of powder composition, morphology and flowability are reported elsewhere [6]. All specimens were fabricated on a Concept Laser M2 Cusing® laser powder bed system using a Yb-fibre laser with 60 µm spot size and a Z-increment (vertical) of 30 µm in an Argon atmosphere with an oxygen-content <0.1%. An island scanning strategy was adopted to balance the residual stresses in the specimens, details of which are given in [6]. After selective melting the islands, laser scans were carried out around the perimeter of the layer with the same process parameters to improve the surface finish. For each subsequent layer, these islands were translated by 1 mm in the X and Y-directions. Since the machine utilised a dimensionless number for hatch spacing (H), instead of scan spacing, H was calculated as scan spacing divided by the laser track width (constant; 150 µm). Following some preliminary SLM trials, mainstream AM structures were built using a full factorial experimental array (24 tests) with varying laser power (P: 200, 250 and 300 W), beam scanning speed (v: 1000 and 1500 mm/s), hatch spacing (H: 0.2 and 0.5) and island size (I: 2 and 5 mm). The optimum processing parameters were selected based on the surface roughness analysis of the SLM cubes.

In the main phase, evaluating the mechanical properties and microstructure of hybrid components, nine tensile dog-bone structures (set-1) were fabricated conforming to BS EN 10 002-

1:1990, see Fig. 1(b). The bottom halves were machined preforms (AA6082-T6), on top of which the other halves were built vertically by SLM (AlSi10Mg). The Fig. 1(a) system was again used. Based on the results from the optimisation trials, a laser power of 300 W, scan speed of 1500 mm/s, hatch spacing of 0.5 and island size of 2 mm were employed during the SLM process. A representative image of the tensile test piece is shown in Fig. 1(c).

Additionally, nine hybrid cylindrical bars (Φ10 × 55 mm) were produced in a similar fashion (Fig. 1(d)), from which dog-bone structures were machined via turning (set-2, Fig. 1(e)). The motive behind this was to compare the mechanical properties before and after heat treatment (HT) of the directly built hybrid specimens with their machined counterparts prepared from the cylindrical bars.

In neither phase was there any preform surface preparation step before SLM, for example for cleaning or oxide removal.

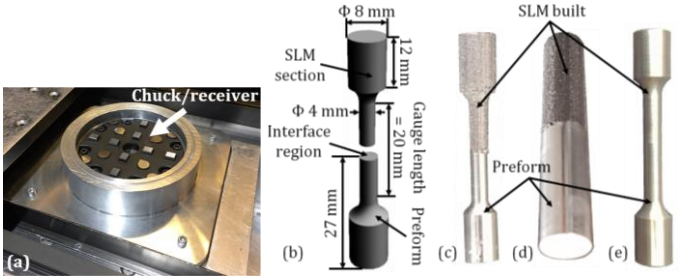

Fig. 1. (a) Modular workpiece holding device, (b) schematic of hybrid tensile specimen, (c) directly built (set-1) test pieces, (d) hybrid cylindrical bars, (e) machined specimens (set-2).

Six of the nine hybrid tensile test pieces from each set (directly built and machined) were subject to annealing/stress relieving at 300 °C for 2 hours [7]. Three out of the six annealed parts were then solution heat treated at 510 °C for 6 hours, followed by water quenching and artificial ageing at 170 °C for 4 hours [8]. The latter condition is hereafter referred to as ST/A.

The surface roughness S_a of the SLM cubes was measured with an Alicona G5 InfiniteFocus microscope, on their top face as well as four side faces. A 1 mm × 1 mm area on each face was scanned using a 20X objective. For S_a of the side faces, an average of four roughness data measured on four side faces of each cube was considered. Minitab 17 software was used for statistical analysis.

Tensile strengths were measured with a ZwickRoell universal testing machine. A pre-load of 100 N and a constant displacement rate of 0.5 mm/min at ambient temperature were set for all tests.

After this, all SLM cubes from the initial phase as well as six hybrid tensile samples (three from each set: as-built, annealed and ST/A) were wire-cut along longitudinal and transverse SLM build directions (LBD and TBD planes, respectively), followed by mounting and mechanical polishing. Both planes of the SLM cubes were scanned using the Alicona microscope (10 × 10 mm) and analysed for determining porosity. Vickers microhardness measurements were carried out on the tensile specimens using a 100 g load and indent time of 15 s. Five measurements were recorded on both planes, and the average was calculated.

In order to reveal microstructure, as-built and heat treated tensile samples were immersion etched in Keller's reagent (2 mL hydrofluoric acid, 3 mL hydrochloric acid, 5 mL nitric acid and 190 mL deionised water) for 45 s and were analysed using a Leica DMLM optical microscope. The specimens were further characterised for grain orientation and texture direction using a Hitachi 3400 SEM based Bruker e-flash electron backscatter diffraction (EBSD) detector at 20kV acceleration voltage, 10 μA current density and 1 μm step size with the images further post-processed using MTEX software.

3. Results and discussion

The main effects of the key SLM parameters on the mean S_a of built parts' top and side faces are presented in Fig. 2(a). Power P has by far the greatest influence, with percentage contribution ratios of 74.5 and 53.8 for top and side faces, respectively, that are statistically significant at 5% significance level. Increasing P reduces S_a on both top and side faces, while increasing scan speed v and island size I increases S_a on the top face but reduces it on the side faces. Hatch spacing H has least effect. Side face S_a was considered to be more important for the tensile test pieces than top face S_a. For least side face S_a SLM parameters were selected as P: 300 W, v: 1500 mm/s, H: 0.5. However I of 2 mm was chosen over 5 mm to render a smoother appearance on the top surface.

Although mean porosity increased with increased laser power (Fig. 2(b)), possibly due to the keyhole effect at higher energy density [9], it decreased with increased levels of the other three factors. Nonetheless, porosity was less than 1% at the optimum operating conditions (at an energy density of 2.67 J/mm²). This is comparable with values reported in [6].

Fig. 3(a) and 3(c) show side and top face topographies of an SLM part processed with P: 200 W, v: 1000 mm/s, H: 0.2 and I: 2 mm, while Fig. 3(b) and 3(d) display those produced using P: 300 W, v: 1500 mm/s, H: 0.5 and I: 2 mm. The extent of unmelted /partially melted powder particles noticed in Fig. 3(a) is much reduced for the trials carried out at higher power (Fig. 3(b)), due to improved remelting of material. Measured S_a are shown inset in each figure part. Side face values reduced from 28 to 7 μm with increased power. Top face values of 10 and 4 μm are less than side face values, though laser scan tracks and island boundaries are clearly visible.

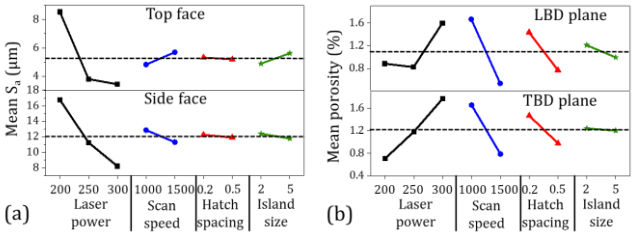

Fig. 2. Main effects of SLM process parameters on (a) surface roughness and (b) porosity of built parts.

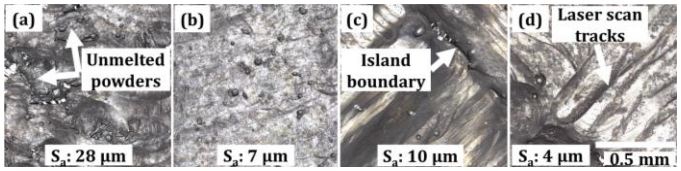

Fig. 3. Representative surface topography of SLM cubes: (a), (b) side and (c), (d) top surfaces.

Images of the broken hybrid tensile test samples and enlarged views at the fractured regions are displayed in Fig. 4. The ultimate tensile strength (UTS) and strain (A^c) data obtained for the directly built specimens and those machined from cylindrical hybrid bars before and after HT are presented in Fig. 5. In each case, the results of all three repetitions are shown. It was observed that all as-built specimens (set-1 and 2) failed at the SM-AM interface under tension. The corresponding UTS varied from 275-364 MPa, which is in agreement with the standard AA6082-T6 property data [4]. Conversely, A^c was much lower, between 2.84-3.85%, compared to that quoted (10%) in [4], possibly due to material's failure at the joint. A disjoined interface in Fig. 6(a) shows the island boundaries while a magnified image

reveals stepped cleavage planes as well as dimples/microvoids (Fig. 6(b)), which is indicative of a mixed brittle-ductile type fracture [10]. This is also consistent with the lower A^c recorded with the as-built hybrid parts.

In contrast to the as-built components, the annealed components failed in the preforms via neck formation (Fig. 4(c)) and the corresponding UTS decreased by 60-61% for both set-1 and 2 specimens. Ductility improved but differently for set-1 and 2, as shown by A^c increasing by 24% (set 1) and 59% (set 2). Equiaxed dimples are observed on the annealed fractured surface, indicating microvoid coalescence, leading to a ductile mode failure (Fig. 6(c)). The ST/A specimens also failed through necking in the preform segments with prominent display of striation marks, although the extent of necking was relatively less compared to the annealed parts (Fig. 4(d)). UTS increased by 102-119% with respect to the annealed state, although it was still lower by ~13-22% from the as-built counterparts. This was however compensated by a higher A^c (~55-72%) compared to those before HT. Both UTS (247-284 MPa) and A^c (4.89-5.61) were somewhat lower than those quoted for AA6082 (~330 MPa and 7%) in [2], the A^c values possibly because they were obtained from the overall gauge length changes, and not from neck cross-sections. Nonetheless, the avoidance of interface failure in the HT specimens suggests improved joint strength and ensures that the HT conditions were adequately chosen. Fractured surfaces of the ST/A samples show signs of ductile mode failure (Fig. 6(d)) although size of the dimples are smaller than those in Fig. 6(c). A further observation is that machined tensile specimens typically exhibited higher UTS and A^c in comparison to the directly built hybrid dog-bone structures. This is possibly due to the better heat distribution over a greater surface area of the set-2 specimens (Φ10 mm) during SLM, compared to the thin cross-section (Φ4 mm) within the gauge length of the set-1 samples, which would have resulted in lower thermal stress distribution in the former.

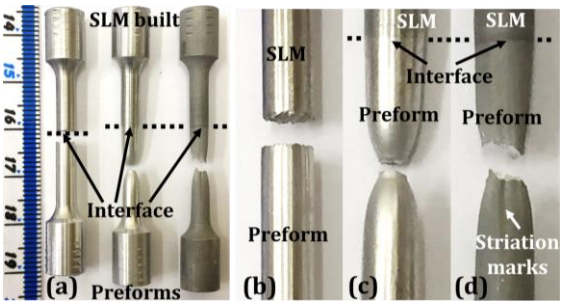

Fig. 4. (a) Images of broken tensile test pieces (set-2), enlarged views at the fractured regions of (b) as-built, (c) annealed and (d) ST/A specimens.

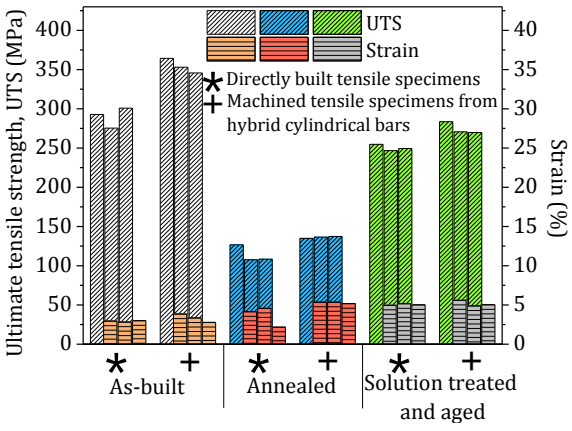

Fig. 5. UTS and A^c of directly built (set-1) and machined hybrid (set-2) tensile specimens before and after HT.

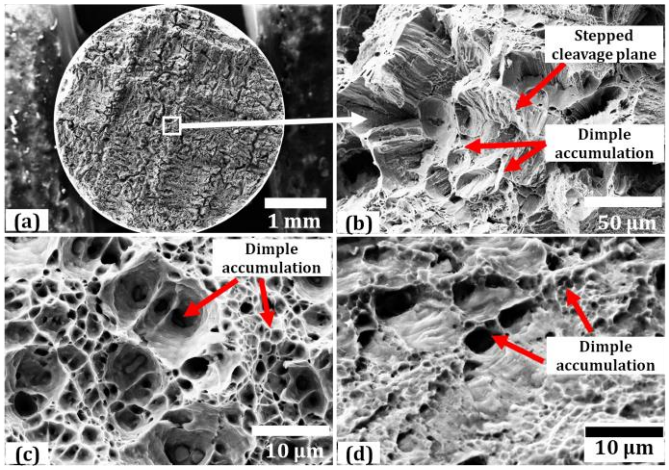

Fig. 6. SEM images showing (a) failure under tension at the interface of as-built specimen, (b) enlarged view at the surface, (c) broken annealed preform surface, (d) solution and aged preform surface after failure.

The Vickers microhardness data of the tensile specimens with and without heat treatment and measured on LBD and TBD planes of both preforms and SLM sections are presented in Fig. 7. Average hardness of the un-heat treated SLM parts (~122-142 $HV_{0.01}$) is in agreement with [10]. The reduction and increase in microhardness follows a similar trend to the UTS before and after HT. The annealed samples exhibited a ~45-55% reduction in microhardness compared to the as-built state. Hardnesses of the ST/A components are typically comparable with the as-built parts, with the exception of the ST/A SLM regions in set-2 samples where microhardness is ~17-24% lower compared to their as-built counterparts. Typically, SLM sections showed higher hardness compared to their preform equivalents, believed to be due to greater Si content (9-10%) in the former material, leading to increased precipitation hardening compared to AA6082 (0.7-1.3% Si) [4]. This at least partly explains the deformation in the preforms during the tensile tests, rather than in the SLM sections after annealing and ST/A. While comparing between the two specimen sets, average hardness of the preforms were similar, whereas the un-heat treated and annealed SLM areas in set-2 displayed ~12-20% higher hardness than set-1 samples. Additionally, hardness values marginally differed when measured on specimens' LBD and TBD planes, except in the case of set-1 solution and aged SLM samples.

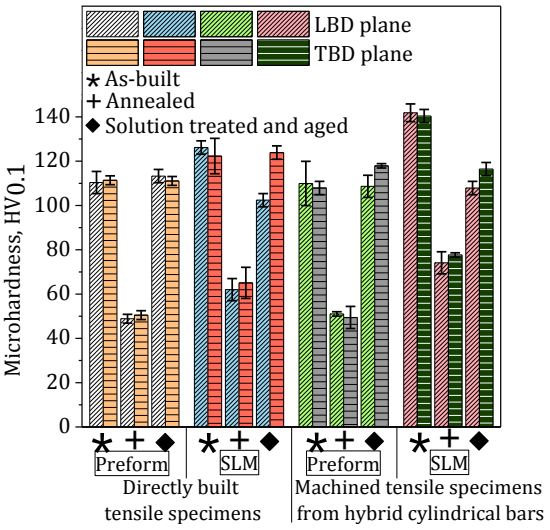

Fig. 7. Microhardness data of hybrid tensile parts before and after HT.

Figure 8(a) reveals interwoven laser scan tracks within the island boundaries on TBD of as-built SLM parts whereas Fig. 8(b) shows coarse cellular zones towards the edge of the boundaries. When viewed on the LBD (Fig. 8(c)), typical fish scale like melt pools of height ~100 µm and width ~200 µm are seen that formed in agreement with the Gaussian distribution of laser energy. Towards the centre of the melt pool, where cooling rates are less than at the edges, fine cellular zones are visible whereas coarser microstructures form near the melt pool edges. The cellular structures are characterised by columnar α-Al dendrites along the built direction and interdendritic eutectic Si particles [11]. Thinner melt pool boundaries are still visible after annealing (Fig. 8(d)), although Si particles become coarser in certain regions, indicating Si phase precipitation within the α-Al matrix.

Melt pool boundaries completely disappear after ST/A. Coarser Si particles are dispersed all over the matrix, together with the formation of a small number of thin, rod-shaped structures which, according to [7], are β-AlFeSi intermetallic phases (Fig. 8(e)). An image taken across the SLM and preform interface of a hybrid tensile test piece shows presence of keyholes (≤125 µm) at the SLM side (Fig. 8(f)), although their presence should not be detrimental to the hybrid parts' fatigue life, as indicated in [12]. Additionally, larger irregular pores in the SLM section are minimal, suggesting adequate remelting of powder particles at optimum SLM parameters. There are also no signs of cracks at the interface. Compared to the distinctive evolution of AlSi10Mg structure following HT, the microstructural change in the preform from the as-received state is less significant, with tiny Si particles randomly scattered in the α-Al matrix after ST/A.

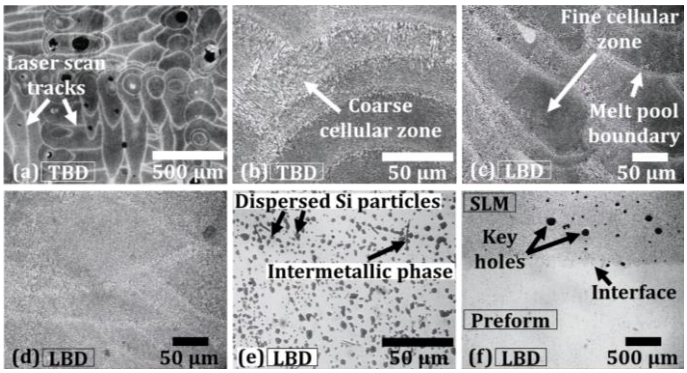

Fig. 8. Microstructures of SLM sections (a), (b), (c) as-built, (d) after annealing, (e) following ST/A, (f) interface microstructure after ST/A.

A mixture of elongated and finer grains is visible in the EBSD image taken on the LBD plane of an as-built SLM region (Fig. 9(a)). Smaller equiaxed grains typically appear at the vicinity of melt pool boundaries while the majority of elongated grains grow along the built direction [7]. The grains start to become larger and more uniform in shape after annealing (Fig. 9(b)).

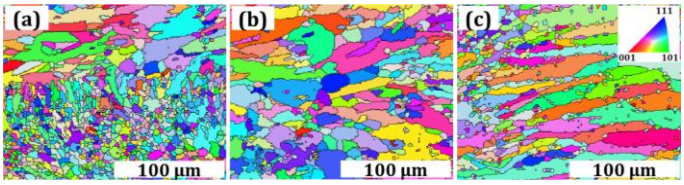

Fig. 9. EBSD inverse pole figures of SLM sections (LBD plane) in the hybrid parts: (a) as-built, (b) after annealing, (c) following ST/A.

Following ST/A, columnar grains with greater width are found, together with tiny particles randomly dispersed all over the matrix (Fig. 9(c)). In contrast to [7], the grains do not exhibit a preferred crystallographic orientation and show a weak texture, regardless of the HT conditions. Thus, the higher hardness of the ST/A SLM samples with respect to the annealed ones is probably due to age hardening by Mg_2Si precipitation [10] that reached the saturation level. This also increases the joint strength between the preform and the SLM regions, leading to failure in the preform section under tension, leaving the interface intact.

4. Conclusions

The present research evaluates mechanical properties and microstructure of hybrid tensile test pieces made from AlSi10Mg SLM structures built on AA6082 preforms. This combination was chosen for its likely application value for lightweight components.

The as-built parts failed under tension at their interface, though at UTS values close to those of fully aged AA6082. After annealing, and after ageing heat treatment, failures always occurred within the AA6082. Thus a process route is opened up for making large parts with small surface features, without the features limiting the strength, by building the small features via SLM, on bigger parts obtained by machining.

Suitable conditions for SLM, from process optimisation trials, are 300 W Yb-fibre laser power, 150 µm track width, 1500 mm/s scan speed, 0.5 hatch spacing and 2 mm island size, for a powder size range of 20-63 µm and a Z-increment of 30 µm. These conditions enable building SLM structures with <1% porosity. After HT, the dispersed Si particles possibly form Mg_2Si phase that strengthens the Al matrix and thus increases the material's microhardness and improves the hybrid parts' joint strength.

Acknowledgements

This project has received funding from the European Union's Horizon 2020 research and innovation programme under the grant agreement No 723826 (MAESTRO).

References

[1] Schmidt M, Merklein M, Bourell D, Dimitrov D, Hausotte T, Wegener K, Overmeyer L, Vollertsen F, Levy GN (2017) Laser based additive manufacturing in industry and academia. *CIRP Annals - Manufacturing Technology* 66:561-583.

[2] Siddique S, Wycisk E, Tenkamp J, Hoops K, Behrens G, Emmelmann C, Walther F (2015) Mechanical performance of hybrid aluminium structures manufactured by combination of laser additive manufacturing and conventional machining processes. *Werkstoffprüfung: Fortschritte in der Werkstoffprüfung für Forschung und Praxis*.

[3] Bourell D, Kruth J-P, Leu M, Levy G, Rosen D, Beese AM, Clare A (2017) Materials for additive manufacturing. *CIRP Annals - Manufacturing Technology* 66:659-681.

[4] Material Property Data for AA6082-T6 (www.matweb.com), *accessed on 16.1.19*.

[5] Penchev P, Bhaduri D, Carter L, Mehmeti A, Essa K, Dimov S, Adkins NJE, Maillol N, Bajolet J, Maurath J, Jurdeczka U (2019) System-level integration tools for laser-based powder bed fusion enabled process chains. *Journal of Manufacturing Systems* 50:87-102.

[6] Read N, Wang W, Essa K, Attallah MM (2015) Selective laser melting of AlSi10Mg alloy: Process optimisation and mechanical properties development. *Materials and Design* 65:417-424.

[7] Takata N, Kodaira H, Sekizawa K, Suzuki A, Kobashi M (2017) Change in microstructure of selectively laser melted AlSi10Mg alloy with heat treatments. *Materials Science & Engineering A* 704:218-228.

[8] Mertens A, Dedry O, Reuter D, Rigo O, Lecomte-Beckers J (2015) Thermal treatments of AlSi10Mg processed by laser beam melting. *Proceedings of the 26th International Solid Freeform Fabrication Symposium*. 1007-1016.

[9] Kempen K, Thijs L, Van Humbeeck J, Kruth J-P (2015) Processing AlSi10Mg by selective laser melting: parameter optimisation and material characterisation. *Materials Science and Technology* 31/8: 917-923.

[10] Li W, Li S, Liu J, Zhang A, Zhou Y, Wei Q, Yan C, Shi Y (2016) Effect of heat treatment on AlSi10Mg alloy fabricated by selective laser melting: Microstructure evolution, mechanical properties and fracture mechanism. *Materials Science & Engineering A* 663:116-125.

[11] Brandl E, Heckenberger U, Holzinger V, Buchbinder D (2012) Additive manufactured AlSi10Mg samples using Selective Laser Melting (SLM): Microstructure, high cycle fatigue, and fracture behaviour. *Materials and Design* 34:159-169.

[12] Tang M, Pistorius PC (2017) Oxides, porosity and fatigue performance of AlSi10Mg parts produced by selective laser melting. *International Journal of Fatigue* 94:192-201.